Journal of Environmental Management 366 (2024) 121712

Contents lists available at ScienceDirect

Journal of Environmental Management

journal homepage: www.elsevier.com/locate/jenvman

Research article

Boosting nutrient recovery from AnMBR effluent by means of electrodialysis technology: Operating parameters assessing

P. Ruiz-Barriga [a,*], J. Serralta [a], A. Bouzas [b], J. Carrillo-Abad [b]

[a] CALAGUA – Unitat Mixta UV-UPV, Institut Universitari d'Investigació d'Enginyeria de l'Aigua i Medi Ambient – IIAMA, Universitat Politècnica de Valencia, Camí de Vera S/n, 46022 Valencia, Spain

[b] CALAGUA – Unitat Mixta UV-UPV, Departament d'Enginyeria Química, Universitat de València, Avinguda de la Universitat S/n, 46100 Burjassot, Valencia, Spain

ARTICLE INFO

Keywords:
Electrodialysis
Nutrient recovery
Urban wastewater
Limiting current
Circular economy
AnMBR

ABSTRACT

This work describes a comprehensive assessment of operating parameters of a bench-scale electrodialysis (ED) plant for nutrient concentration from an Anaerobic Membrane BioReactor (AnMBR) effluent. The ED bench-scale plant serves a dual purpose. Firstly, to generate a concentrated stream with a high nutrient content, and secondly, to produce high-quality reclaimed water in the diluted stream, both sourced from real wastewater coming from the effluent of an AnMBR. Two sets of experiments were conducted: 1) short-term experiments to study the effect of some parameters such as the applied current and the type of anionic exchange membrane (AEM), among others, and 2) a long-term experiment to verify the feasibility of the process using the selected parameters. The results showed that ED produced concentrated ammonium and phosphate streams using a 10-cell pair stack with 64 cm^2 of unitary effective membrane area, working in galvanostatic mode at 0.24 A, and operating with an Acid-100-OT anionic exchange membrane. Concentrations up to 740 mg/L and 50 mg/L for NH_4–N and PO_4–P, respectively, were achieved in the concentrated stream along with removal efficiencies of 70% for ammonium and 60% for phosphate in the diluted stream. The average energy consumption was around 0.47 $kWh \cdot m^{-3}$.

1. Introduction

Nitrogen (N) and phosphorus (P) are nowadays highly demanded elements for fertilizer production. Indeed, the recovery and valorisation of these resources, for subsequent application in agriculture, has been gaining attention within the wastewater treatment sector. This is related to the high amounts of nutrients (mainly N and P) present in wastewaters (WW). Moreover, their removal from WW is a crucial step that must be carried out in sensitive areas due to the great impact they can cause. Therefore, the development of efficient processes allowing nutrients extraction from wastewater becomes crucial for the environment. In this sense, several technologies have been investigated for the elimination and recovery of these nutrients, from traditional methods such as absorption (Ukwuani and Tao, 2016), chemical precipitation (He et al., 2013; Ye et al., 2017) or reverse osmosis (Luo et al., 2016; Vega et al., 2022) to currently popular technologies such as microalgae cultivation (González-Camejo et al., 2018; Herrera et al., 2021), which can retain high amounts of ammonium and phosphate. Furthermore, membrane contactors (Darestani et al., 2017; Noriega-Hevia et al., 2020; Rongwong and Goh, 2020), struvite precipitation (Pastor et al., 2009; Sena and Hicks, 2018), bioelectrochemical systems (Osset-Álvarez et al., 2019; Raychaudhuri and Behera, 2021) and electrochemical systems (Luther et al., 2015; Ward et al., 2018) are the subject of extensive research and application in the field of nutrient recovery from urban wastewaters.

Electrodialysis (ED) has been used as an ion concentration method for more than 50 years, mainly to obtain drinking water from brackish water (Strathmann, 2010). Nowadays its use has also been spread out to urban and industrial wastewater treatment. ED is an electrochemical membrane process based on the application of an electrical field as the electromotive force to separate and/or concentrate anions and cations by alternating anion and cation exchange membranes (Strathmann, 2010; Xie et al., 2016; T. Yan et al., 2018). The main advantages of ED technology are a high recovery rate and low energy consumption compared to other membrane-based technologies, long membrane lifetime and high selectivity, allowing a selective separation of ions and thus, the concentration of target nutrients as ammonium or phosphate (Al-Amshawee et al., 2019; Sedighi et al., 2022). However, the main disadvantages of this technology, common to most membrane processes, are fouling and scaling (Nthunya et al., 2022; Singh and Hankins, 2016; H. Yan et al., 2018).

* Corresponding author.
E-mail address: patruiba@iiama.upv.es (P. Ruiz-Barriga).

https://doi.org/10.1016/j.jenvman.2024.121712
Received 9 March 2024; Received in revised form 31 May 2024; Accepted 2 July 2024
Available online 13 July 2024

In recent years, significant advances have been made in the field of WW treatment with ED technology. Zhang et al. (2013) worked on a selective ED process intending to increase the efficiency of phosphate recovery in the effluent of a struvite crystallization reactor reaching recovery efficiencies up to 93%. On the other hand, Tarpeh et al. (2018) worked with a lab-scale system that combined ED with a hydrophobic membrane to recover ammonia from urine as ammonium sulphate with recovery efficiencies up to 93% after 24 h of operation with an energy consumption of 30,6 MJ kg^{-1} N. Ye et al. (2019) developed an ED method for fractioning and concentrating ions from synthetic WW into three different product streams by the use of monovalent selective anionic and cationic exchange membranes. These streams were finally paired to obtain valuable products such as calcium phosphate ($Ca_3(PO_4)_2{\cdot}xH_2O$) and magnesium phosphate ($Mg_3(PO_4)_2{\cdot}yH_2O$). Ward et al. (2018) used a 30-cell pair pilot scale stack to concentrate ions from an anaerobic digestor supernatant achieving NH_4–N concentrations 8 times higher than initial ones and with an energy consumption of 4.9 ± 1.5 $kWh{\cdot}kg^{-1}$ NH_4–N. Hence, the emerging ED process combined with other technologies is a highly promising method for nutrient recovery and subsequent valorisation.

On the other hand, Anaerobic Membrane Bioreactors (AnMBRs) are recognized for their energy-efficient and cost-effective nature, consuming less energy compared to aerobic-based processes. This results in a reduced volume of biosolids for management and the conversion of biodegradable organics into methane (CH_4), a gaseous energy carrier suitable for energy production (Robles et al., 2018). However, the effluent of an AnMBR system contains substantial quantities of N and P since organic N and P are mineralized into NH_4–N and PO_4–P. These NH_4–N and PO_4–P effluent concentrations might hinder the direct discharge into different receiving water bodies or even possible fertigation applications. In those cases, AnMBR must be combined with a complementary post-treatment process to fulfil two purposes: i) achieving required discharge limits (15 mg N/L and 2 mg P/L between 10,000 p.e (population equivalent) and 100,000 p.e, and 10 mg N/L and 1 mg P/L for more than 100,000 p.e, according to Council Directive 91/271/EEC) and ii) promoting nutrient recovery by means of the aforementioned technologies where NH_4–N and PO_4–P preconcentration stages would be required for increasing recovery efficiencies. In that point, ED could be coupled to AnMBR technology helping to shift WW treatment towards circular economy. Despite this, there are few studies in which real WW has been used as feeding solution of ED stacks (Mohammadi et al., 2020; Voutetaki et al., 2023; Yang et al., 2023). In fact, among these studies no one explored the use of AnMBR effluent coupled with ED technology and thus, there is a lack of information concerning the utilization of ED for nutrient concentration from AnMBR effluents.

Thus, while there have been notable strides in the field, a comprehensive assessment of the operating parameters concerning the utilization of ED for nutrient concentration from AnMBR real effluent remains pending. Moreover, the identification of optimal operational strategies within ED systems still lacks clarity. Therefore, this work focuses on determining the suitable configuration of an ED stack treating an AnMBR effluent to obtain i) a high NH_4–N and PO_4–P concentrated stream, to boost the efficiency of subsequent nutrient recovery processes, which are not developed in this work, and ii) high quality reclaimed water. A bench-scale study has been performed to establish the optimal configuration of the ED assessing the optimal parameters such as the current density, the suitable type of anionic membrane, the number of cell pairs and the power supply operation mode, in terms of energy consumption and removal and recovery efficiencies.

2. Materials and methods

The work was performed at lab-scale. The following paragraphs summarise the experimental procedure of the ED experiments carried out in this paper.

2.1. Feed water

Effluent from an AnMBR pilot plant was used as feed water of the ED process. The AnMBR pilot plant was located at the Conca del Carraixet WWTP (Valencia, Spain) and was fed with WW coming from the WWTP. AnMBR effluent average concentrations during the experimental period are shown in Table 1. Sulphur was not detected in the effluent of the AnMBR during the ED experiments due to their conversion to sulphate during the storage period prior its use in the ED stack.

2.2. ED system and experimental procedure description

In the following sections, the ED equipment and the experimental procedure are explained. The analytical methodology and performance indicators for calculations are also described.

2.2.1. Experimental set-up

The equipment used in this study was supplied by PCCell GmbH (Germany) and consisted of a laboratory ED stack (64-002) linked to pumping units (BED 1–2) which allows working with a maximum of 10-cell pairs and with a unitary flow around 5 L/h. The stack was composed of four loops leading to a concentrated stream, a diluted stream and two electrolyte streams. The same electrolyte was recirculated as anolyte and catholyte since the formation of products in the anodic and cathodic chambers were not the objective of this work. BED 1–2 consisted of two conductivity meters and two temperature sensors (CTI-500, JUMO GmbH & Co, Germany) for both concentrated and diluted streams. Flow meters for concentrated, diluted and electrolyte streams (DFM 165, Stubbe GmbH & Co, Germany) were also included. Pumps for both diluted and concentrated solutions (NPD 14/12, ITS-Betzel, Germany), equipped with a diaphragm valve for flow control (Gemu 617, GmbH & Co, Germany), were used to provide a flow rate from 0 L/h to 100 L/h. Additionally, an electrolyte pump (NPD 14/12, ITS-Betzel, Germany) was employed. A 0.2 μm pore-size cartridge filter was placed prior to the ED cell to prevent membrane fouling due to solid accumulation. The concentrated and diluted tanks had a capacity of 2 L and the electrolyte solution tank had a maximum capacity of 5 L. The system allows working with automatic hydraulic control and all parameters were shown at the PC Frontend display. A stable current/voltage was supplied by a Voltcraf PPS-11815 power supply (Conrad Electronics, Germany) with a maximum voltage of 36 V and a maximum current of 5A. The ED stack was composed of both Ti/RuO_2 anode and cathode with an area of 64 cm^2.

Four types of membranes (11.0 × 11.0 cm) were used during the experimental tests. PC-SK cation exchange membranes (CEM) and Acid-100, Acid-100-OT and Acid-60 anion exchange membranes (AEM) were used. All membranes had an active area of 64 cm^2 and spacers used to build diluted and concentrated streams were made of polypropylene with a 0.45 mm thickness. The main characteristics of membranes also provided by PCCell GmbH (Germany) are shown in Table S1 (Supplementary Material).

Table 1
Average of AnMBR effluent concentrations.

	AnMBR effluent		
pH	6.82	±	0.11
Conductivity (mS/cm)	1.81	±	0.43
Alkalinity (mg $CaCO_3$/L)	642.1	±	97.4
DQO_{sol} (mg/L)	61	±	25.2
NH_4–N (mg/L)	56.0	±	5.2
PO_4 -P (mg/L)	8.1	±	1.5
SO_4–S (mg/L)	122.4	±	46.6
Cl^- (mg/L)	263.5	±	53.7
Na^+ (mg/L)	126.1	±	18.5
K^+ (mg/L)	13.1	±	3.4
Mg^{2+} (mg/L)	43.7	±	4.1
Ca^{2+} (mg/L)	165.9	±	10.9

2.2.2. Experimental procedure

In all experiments, 2 L and 1.5 L of AnMBR effluent were fed to the diluted and concentrated tanks, respectively, and 2 L of H_2SO_4 0.01 M was used as supporting electrolyte. The stack configuration was CEM/AEM for n-cell pairs (for n = 1, 5 or 10) using n+1 CEM and n AEM. Three different set of experiments were performed: chronopotentiometry tests, short-term experiments, and a long-term experiment.

First, chronopotentiometry tests were performed from 0.1 A to 1.2 A using PC-SK and Acid-100 membranes. The corresponding steady state voltage of each current value tested was obtained for polarization curve determination. For these experiments, diluted and concentrated streams were passed through the ED stack only once, with the aim of not producing changes in the feed solution, and obtaining the steady state voltage values.

Thereafter, short-term experiments were carried out to study the effect of different parameters in the ED process. (i) Current applied: a 1-cell pair stack was used, and an Acid-100 anionic exchange membrane and two PC-SK cationic exchange membranes were selected. Four current values were applied: 0.48 A, 0.40 A, 0.33 A and 0.24 A corresponding with current density values of 75.0 A m^{-2}, 62.5 A m^{-2}, 51.6 A m^{-2}, 37.5 A m^{-2}, respectively; (ii) Type of anionic membrane: three different membranes (Acid-100, Acid-100-OT and Acid-60) were assessed applying 0.24 A and using 1-cell pair stack; (iii) Number of cell pairs: 1, 5 and 10-cell pairs were assessed also applying 0.24 A and using Acid-100-OT and PC-SK anionic and cationic exchange membranes, respectively. The flow rate was 5 L/h, 25 L/h and 50 L/h in 1, 5 and 10-cell pairs, respectively. (iv) Power supply operating mode: three different values of voltage were applied – 7.5 V, 10 V and 12.5 V – to compare the potentiostatic operating mode (CV) with the galvanostatic mode (CC) assessed in previous experiments at 0.24 A. All these experiments were performed in semi-batch mode since the concentrated stream was recirculated to the feed tank until the end of the experiment, and the diluted stream was recirculated during a cycle and renewed when the cycle finished. During experiments, prolonged voltages above 22 V were avoided to prevent membrane damage (Ye et al., 2019), and thus, when this voltage was reached in the ED stack, one cycle was completed, and new feed water was introduced in the diluted tank. The end of a short-term experiment was determined either by a fixed number of cycles or by a predetermined total duration of the experiment. An overview of the short-term experimental conditions is shown in Table S2 (Supplementary Material).

Finally, a long-term experiment with 10-cell pair stack configuration was carried out. The optimal parameters established in the previous short-term experiments – i.e., current, type of anionic membrane, number of cell pairs and operating power supply mode – were employed. The experiment was performed in order to accomplish two purposes: (i) to reach the discharge limits set in Directive 91/271/ECC at the diluted stream, allowing a maximum voltage of 22 V to avoid membrane damaging; (ii) to reach NH_4–N and PO_4–P concentration levels for enabling subsequent recovery stages in membrane contactors and in struvite crystallization processes (Desmidt et al., 2013; Mehta et al., 2015; Noriega-Hevia et al., 2020; Salehi et al., 2018; Tansel et al., 2018). When target values in concentrated stream were achieved an entire experiment was completed.

In all experiments, the pH of the concentrated stream was maintained below 4.5 to prevent calcium phosphate precipitation, achieved through the addition of low doses of 37% hydrochloric acid. Samples of each stream for later analyses were taken at the beginning, middle and final of each cycle in all experiments. Voltage, current, temperature and conductivity of both concentrated and diluted streams were continuously recorded. In short-term experiments, only NH_4–N and PO_4–P concentrations are shown, whereas in the long-term experiment, values for sulphate, calcium, magnesium and potassium are also included due to the relevance of the competing ions in larger duration experiments.

2.3. Analytical methods

All samples were analysed by an ion chromatograph (IC) (883 Basic IC Plus, Metrohm, Switzerland). The anion column (Metrosep A supp 5250/4, Metrohm, Switzerland) employed a solution of 3.2 mM Na_2CO_3/1.0 mM $NaHCO_3$ as eluent with a flow rate of 0.7 ml/min and H_2SO_4 200 mM as chemical suppressor. The cation column (C4 150/4, Metrohm, Switzerland) worked with 1 mM oxalyc acid and 3 mM HNO_3 eluent with a flow rate of 0.9 ml/min pH in concentrate, dilute and electrolyte streams and conductivity in the electrolyte stream were measured for each sample with a pH meter (Sentix® 41, WTW) and a conductivity meter (TetraCon® 325, WTW), respectively. Experiments were performed at room temperature (22±2 °C).

2.4. Performance indicators

Energy consumption was determined using equation (1). Once the energy consumption was obtained for each experiment, it was expressed per volume (m^3) of treated water (2) or per kg of NH_4–N or PO_4–P recovered (3).

$$E = \int_0^t U \cdot I \cdot dt \tag{1}$$

$$E = \frac{\left(\int_0^t U \cdot I \cdot dt \right)}{V} \tag{2}$$

$$E = \frac{\left(\int_0^t U \cdot I \cdot dt \right)}{m} \tag{3}$$

Where E is the energy consumption in kWh, I is the applied current at time t in ampers (A), U is the cell voltage reached at every instant of time in volts (V), V is the volume of treated water expressed in cubic meter and m is the mass of NH_4–N or PO_4–P recovered in the concentrated stream expressed in kilograms.

Efficiencies of diluted and concentred streams were calculated by equations (4) and (5).

$$\eta_{removal}\ (\%) = \frac{m_{inlet} - m_{dil\,t=f}}{m_{inlet}} \cdot 100 \tag{4}$$

$$\eta_{recovery}\ (\%) = \frac{m_{conc\,t=f} - m_{conc\,t=i}}{m_{inlet} - m_{dil\,t=f}} \cdot 100 \tag{5}$$

Here m_{inlet} represents the total mass of the corresponding ion in the inlet stream, $m_{dilt=f}$ and $m_{conct=f}$ are the total final mass of the corresponding ion in the diluted and the concentrated stream, respectively, and $m_{conct=i}$ is the total initial mass of the corresponding ion in the concentrated stream. All quantities were expressed in grams considering all cycles conducted. Equations were adapted from Tarpeh et al. (2018).

Dilution and concentration ratios were calculated by equations (6) and (7).

$$F_D = \frac{\overline{C}_{inlet}}{\overline{C}_{dil.\,t=f}} \tag{6}$$

$$F_C = \frac{C_{conc.\,t=f}}{\overline{C}_{inlet}} \tag{7}$$

Where $\overline{C}_{inlet}$ is the average inlet concentration, $\overline{C}_{dil.\,t=f}$ is the average concentration of the diluted stream at the end of each working cycle, and $C_{conc.\,t=f}$ is the final concentration of the experiment in the concentrated compartment. This parameter explains the increase or the decrease of the inlet concentration at the end of the experiment in the concentrated or diluted stream, respectively.

Finally current efficiency (CE) for a determined ion was calculated in long-term experiment by equation (8).

$$CE_A\ (\%) = \frac{z \cdot \frac{m_{conct=f}}{M_A} \cdot F}{N \cdot I \cdot t_f} \cdot 100 \quad (8)$$

Where z is the charge of the ion A, M_A is the molar mass of the ion A, F is the faraday constant (96,485 C/mol), N is the number of cell pair, I is the current applied in ampers and t_f is the duration of the experiment in seconds. The total CE was calculated by the sum of the different CE obtained for each ion.

3. Results and discussion

Three sets of experiments were carried out in this work. First, chronopotentiometries tests were performed for polarization curve determination. Thereafter, short-term experiments were conducted to study the effect of the operating parameters of the process. Finally, a long-term experiment was carried out to demonstrate the feasibility of ED to treat and concentrate nutrients from real wastewater.

3.1. Limiting current determination

Limiting current (LC) was determined to establish the optimal current for ED operation. Different chronopotentiometries were tested using currents from 0.1 A to 1.2 A (Fig. 1A) and the corresponding steady state voltage (U_m) for each current was represented given rise to the polarization curve of the system (Fig. 1B). Useful information can be extracted from the analyse of the chronopotentiometry tests, especially from the diffusion boundary layer (DBL) of the diluted compartment (Martí-Calatayud et al., 2018a). An increase in the voltage drop of the membrane system is manifested when a depletion of ions in the diluted DBL is experimented (Martí-Calatayud, 2015) No, 1991; Nthunya et al., 2022; Parulekar, ; Yan et al., 2018. On the other hand, the concentrated compartment will experiment a growth of the DBL due to the accumulation of ions on the surface of the membrane. This also led to the increase of the resistance of the system, due to a possible scaling phenomenon. Regarding Fig. 1A, values around 0.80 A experimented a higher increase in voltage for the same increment in current (0.1 A). This could be associated, as explained above, with the decreased of ions near the surface of the membrane (DBL) and thus, the increase in the resistance of the stack and in consequence, the increase in drop voltage. In Fig. 1B the polarization curve is examined and a well-defined change in slope between the first linear region and the second one is identified at 0.87 A, corresponding, approximately, with the increase in voltage at 0.8 A in Fig. 1A. The second region shows a slope decrease compared to the first region. Thus, the first region (up to 0.87 A) is defined as the ohmic region, and the second one as the plateau region, even though the plateau region does not adhere to the typical trend defined in theory (a marked region with a slope near zero) (Cerva et al., 2018). The over-limiting region could not be determined due to the limitations of the power supply. To confirm the determined LC value in the polarization curve, the method proposed by Isaacson and Sonin (1976) and the method proposed by Cowan and Brown (1959) were applied to the obtained values (Fig. S1, Supplementary Material). This resulted in a current of 0.81 A for both methods.

The LC of the system, resulting from the average value obtained from both methods and the polarization curve, was set to 0.84 A. The ED stack is usually operated below the LC value, in order to decrease the energy costs of the system (Martí-Calatayud et al., 2018a). According to Strathmann (2010), optimal ED operation can be performed between 60 and 80% of the LC. In the present work approximately 60% of this value was chosen, resulting in a current of 0.48A.

3.2. Effect of the current applied

Despite the determined working current of 0.48 A, four different values of current between the ohmic and the plateau region (0.48 A, 0.40 A, 0.33 A, and 0.24 A) were tested to assess the effect of this parameter on the ED process. Fig. S2 shows the evolution of the voltage during the different experiments, showing that the only experiment where voltage remains at the same value at the beginning of each new cycle was the one performed at 0.24 A. However, in the 0.48 A, 0.40 A and 0.33 A experiments (Fig. S2), the initial voltage was not stable increasing steeply at the beginning of each new cycle and reaching voltages close to the critical one (22 V) very quickly. This could be associated with an increase in the ions concentration near the DBL on the concentrated side of the membranes, leading to an increment in the thickness of the DBL and resulting in scaling formation (Martí-Calatayud et al., 2018b). This, in turn, could result in an increase of the system resistance leading to a higher cleaning frequency of the stack and to a higher frequency of system shutdown. Table 2 shows the concentrations obtained in the diluted and concentrated streams as well as the calculated dilution and concentration ratios. Experimental times were around 650 min in all cases.

It was expected to obtain higher concentration and dilution ratios as the current was increased. On one hand, in the concentrated stream, the higher the applied current, the greater the final concentrations for both ammonium and phosphate, thus, increasing the concentration ratio. This can be explained by the fact that higher current values promoted ion migration but also accelerated the polarization phenomenon in the DBL, consequently leading to shorter cycles and, thus, to a higher volume treated within the same operating time. On the other hand, the dilution ratio decreased as the current applied increased for both ammonium and phosphate, following a different trend from expected. This was associated with scaling formation phenomena at higher current values that led to shorter cycles and finally, to the process shutdown due to critical voltages being reached. Furthermore, when low current values are applied, the lower migration velocities result in a delay in the growth of the DBL lengthening the cycles duration and allowing more ions to migrate from diluted stream to the concentrated one. However, for the

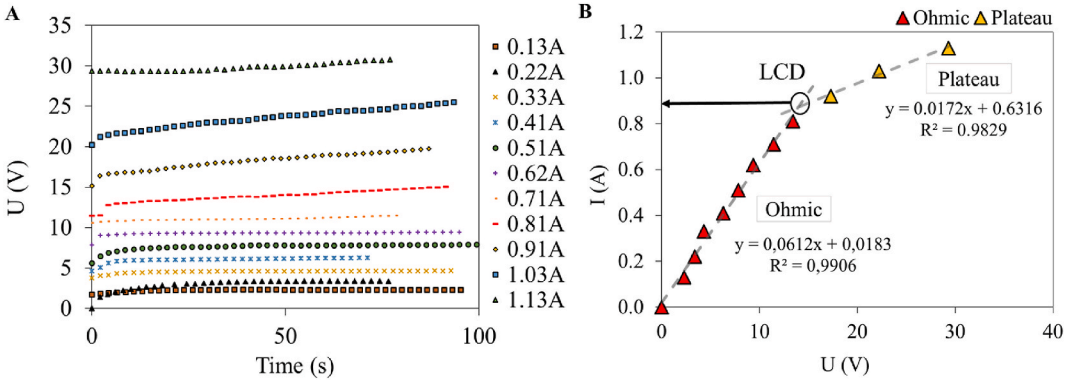

Fig. 1. LCD determination. A) Chronopotentiometry tests from 0.1 A to 1.2 A. B) Current vs Voltage method.

Table 2
Effect of the applied current on process performance.

	Current (A)	Concentration (mg/L)							Ratio	
		Inlet			Diluted			Concentrated	Dilution	Concentration
NH_4–N	0,48 A	49.99	±	0.77	15.59	±	6.87	267.61	3.2	5.4
PO_4–P		4.22	±	0.72	2.84	±	0.51	23.54	1.5	5.6
NH_4–N	0,40 A	53.09	±	0.08	11.73	±	5.76	142.47	4.5	2.7
PO_4–P		4.80	±	0.14	2.92	±	0.37	17.13	1.6	3.6
NH_4–N	0,33 A	54.02	±	1.44	6.79	±	3.41	138.32	8.0	2.6
PO_4–P		7.16	±	0.67	3.04	±	0.40	16.05	2.4	2.2
NH_4–N	0,24 A	47.81	±	0.23	8.35	±	1.50	78.24	5.7	1.6
PO_4–P		10.16	±	0.29	2.76	±	0.23	19.02	3.7	1.9

same operating time, less amount of N and P were added to the system at low current values since fewer cycles were performed, resulting in lower concentration ratios. Particularly, the dilution ratio for ammonium at 0.33 A (8.0) exceeds the one obtained at 0.24 A (5.7). This was attributed to the higher current of the 0.33 A experiment compared to the 0.24 A and to the fact that scaling in the 0.33 A was lower than in the 0.48 A and 0.40 A experiments. This behaviour was not observed in the case of phosphate since this ion presented lower migration velocities (Table S3) needing longer cycle duration to migrate from diluted to concentrated stream.

In relation with removal and recovery efficiencies (Fig. 2A and B), the behaviour observed for the ammonium was similar to the one obtained for the dilution and concentration ratios, respectively. The removal efficiencies for phosphate also followed the same trend that the ones observed for the corresponding dilution ratios. However, the recovery efficiencies for phosphate exhibited an increase as the applied current decreased (Fig. 2B), showing recovery values of 51% for phosphate at 0.24 A. This was attributed to the lower current values that favour the migration of ions from diluted towards concentrated compartment.

Regarding energy consumption (Fig. 2C and D), the lowest values were obtained at 0.24 A yielding 1.55 kWh·m^{-3}, 68.5 kWh·kg^{-1} NH_4–N and 281.7 kWh·kg^{-1} PO_4–P. The lower energy consumption per treated volume observed at 0.48 A, compared to the ones obtained at 0.40 A and 0.33 A experiments, can be attributed to the number of cycles performed in this experiment. At 0.48 A, more cycles were completed, resulting in the treatment of a higher volume and thus the introduction of higher amounts of ammonium and phosphate into the system. This led to similar energy consumption per recovered kilogram of ammonium and phosphate and lower values in terms of the volume of treated water, despite the higher current and voltage applied. Considering the observed instability when the system operates at current values exceeding 0.24 A (Fig. S2), and the better results achieved in terms of removal and recovery efficiency (overall for phosphate) and energy consumption at 0.24 A, this current value was set as the most suitable for the studied system.

It is important to note that in the diluted stream, discharge limits for the less restrictive criteria (i.e., 15 mg/L of NH_4–N and 2 mg/L of PO_4–P between 10,000 p.e. and 100,000 p.e; Directive 91/271/EEC) were reached for ammonium (excepting at 0.48 A experiment) but not for phosphate in any experiment.

3.3. Effect of the AEM type

Table 3 shows the inlet, diluted and concentrated stream concentrations for the three studied membranes. For a better comparison, a similar experimental duration (i.e., approximately 600 min) was used for the three different experiments.

The Acid-100-OT membrane exhibited the highest concentrations in the concentrated stream, reaching 125.11 mg NH_4–N/L and 25.59 mg

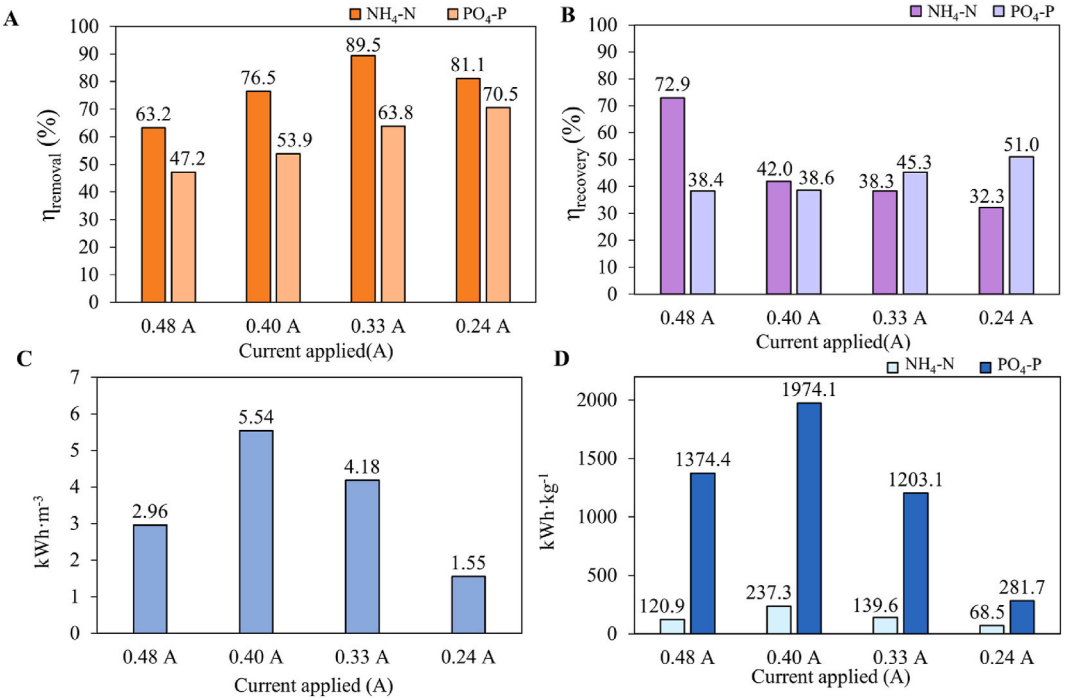

Fig. 2. Removal efficiency (A), recovery efficiency (B) and energy consumption (C and D) for the four current values applied (0.48A, 0.40A, 0.33A and 0.24A).

Table 3
Effect of the Acid-100, Acid-100-OT and Acid-60 anionic exchange membranes on process performance.

	AEM	Concentration (mg/L)							Ratio	
		Inlet			Diluted			Concentrated	Dilution	Concentration
NH_4–N	Acid-60	47.81	±	0.23	4.28	±	2.31	76.75	11.2	1.6
PO_4–P		10.16	±	0.29	3.31	±	1.93	15.48	3.1	1.5
NH_4–N	Acid-100	47.81	±	0.23	8.35	±	1.50	78.24	5.7	1.6
PO_4–P		10.16	±	0.29	2.76	±	0.23	19.02	3.7	1.9
NH_4–N	Acid-100-OT	54.57	±	0.22	2.49	±	1.35	125.11	21.9	2.3
PO_4–P		10.16	±	0.18	2.59	±	0.50	25.59	3.9	2.5

PO_4–P/L. Concentrations below discharge limits were achieved in the diluted stream for ammonium. However, none of the cases met the criteria for phosphate, approaching the less restrictive limit set by Directive 91/271/EEC (2 mg P/L) when using the Acid-100-OT membrane. The higher concentrations of ammonium and phosphate observed with the Acid-100-OT membrane were associated with a greater number of cycles within the same operating time, introducing a larger quantity of these elements into the system. The Acid-100-OT membrane also showed the highest dilution and concentration ratios for both ammonium and phosphate.

The removal efficiencies (Fig. 3A) were similar for the three AEM tested showing values between 80% and 90% for ammonium and 65% and 70.5% for phosphate. However, the recovery efficiencies (Fig. 3B) were significantly higher when using the Acid-100-OT membrane with values of 60.3% for phosphate and 39% for ammonium. Considering the lowest resistance of the Acid-60 membrane (~2 Ω cm^2, Table S1) – suitable for longer operation times per cycle, as it would reduce the stack resistance – no significant improvements were observed compared to Acid-100 and Acid-100-OT membranes. Conversely, the Acid-100-OT membrane showed a lower resistance (~4 Ω cm^2), in contrast to Acid-100 (~5 Ω cm^2), contributing to the increased recovery efficiencies. On the other hand, the Acid-60 membrane showed the highest energy consumption (Fig. 3C and D). Acid-100 and Acid-100-OT membranes showed similar energy consumptions as expected due to its similar resistances. The lowest energy consumption of Acid-100-OT (1.48 kWh·m^{-3}, 57.5 kWh·kg^{-1} of NH_4–N and 281.1 kWh·kg^{-1} of PO_4–P), the highest recovery efficiency and the similar removal efficiency among the studied membranes made the Acid-100-OT themost appropiate one for the process under study.

3.4. Effect of the number of cell pairs

Once the suitable membrane type was chosen, the number of cell pairs was assessed to optimize the removal and recovery efficiencies as well as the energy consumption in the process. Three experiments were performed working with 1, 5 and 10-cell pairs using an Acid-100-OT membrane at 0.24 A. Table 4 shows the concentrations achieved in each experiment after 4 cycles of operation. The total experiment duration (i.e., 750, 190 and 92 min for 1, 5 and 10-cell pairs, respectively) decreased due to the higher flowrate (5 L/h, 25 L/h, and 50 L/h, respectively).

In the concentrated stream, ammonium concentration remained almost constant across the three experiments performed, while phosphate concentration was similar for 5 and 10-cell pair assays but doubled in the single cell pair experiment. This increase was attributed to the higher initial phosphate concentrations in the single cell pair experiment (10.28 mg PO_4–P/L) compared to concentrations close to 6 mg PO_4–P/L for 5 and 10-cell pairs experiments. As for the concentration values, the concentration ratio remained stable for both ammonium and phosphate in all the experiments conducted. In the diluted stream,

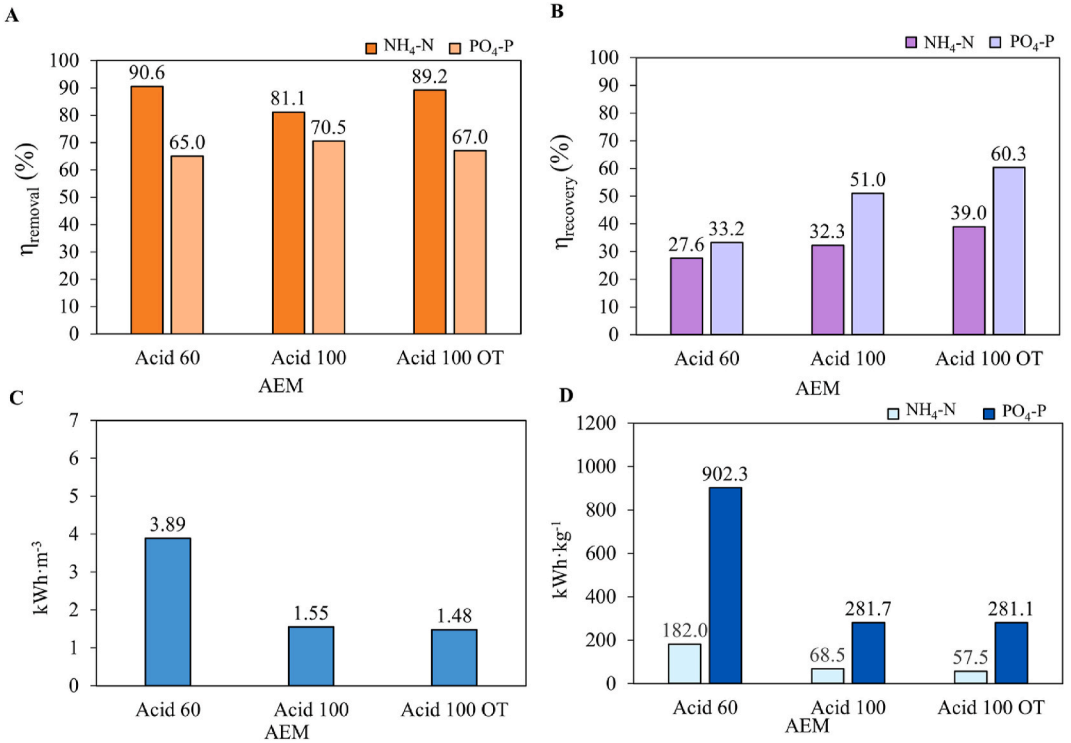

Fig. 3. Removal efficiencies (A), recovery efficiencies (B) and energy consumption (C and D) for the three AEM tested (Acid-60, Acid-100 and Acid-100-OT).

Table 4
Effect of the number of cell pairs on process performance.

	Cell pair	Concentration (mg/L)							Ratio	
		Inlet			Diluted			Concentrated	Dilution	Concentration
NH_4–N	1	54.64	±	0.35	2.75	±	1.21	184.09	19.9	3.4
PO_4–P		10.28	±	0.19	2.64	±	0.42	30.89	3.9	3.0
NH_4–N	5	50.54	±	0.18	5.88	±	0.81	167.68	8.6	3.3
PO_4–P		6.13	±	0.00	2.04	±	0.07	18.29	3.0	3.0
NH_4–N	10	51.07	±	0.45	8.41	±	0.40	191.17	6.1	3.7
PO_4–P		6.17	±	0.06	2.18	±	0.04	17.33	2.8	2.8

concentrations for ammonium increased with the raise in cell pairs, whereas phosphate concentrations remained nearly constant across the different assays. The increase in the ammonium concentrations in the diluted stream was associated with a shorter cycle time – due to a higher flowrate –, leading to a lower migration of ions from the diluted to the concentrated compartment. However, the similar phosphate concentration across different tests in the diluted stream was attributed to the low migration velocities of this ion (Table S3). Specifically, with a single cell pair, ammonium dilution ratio was 19.9, while it was 8.6 and 6.1 for 5 and 10 cell pairs, respectively. Regardless, the P limit values set by European regulations were not met at any experiment. This represents a current bottleneck that will be addressed in future research. Notably, other researchers have explored alternative approaches, such as a multistage configuration using several serial ED cells to obtain higher concentration and dilution efficiencies (Simões et al., 2022; H. Yan et al., 2018).

Concerning removal efficiencies (Fig. 4A), it is noteworthy that there was a declining trend in dilution efficiencies as the number of cell pairs increased, observed for both NH_4–N and PO_4–P values. As expected, this trend can be attributed to the rise in the system resistance, resulting in a higher initial voltage requirement. Consequently, the predetermined voltage limit (set at 22 V) was reached earlier, leading to higher final concentrations in the diluted stream compared to those obtained with 1 and 5-cell pairs. In opposite, the assay with 10-cell pairs exhibited the highest recovery efficiencies for ammonium and quite similar phosphate recovery efficiency than the one obtained for the 5-cell pair (Fig. 4B). Nonetheless, considering that the time required to achieve those recovery efficiencies was lower for the 10-cell pair configuration, it is evident that the 10-cell pair yields notably superior results compared to the 1 and 5-cell pair configurations.

As expected, an increase in the number of cell pairs resulted in a higher volume of treated water, leading to a significant reduction in energy consumption per unit of treated water and also in energy consumption per kg of N and P recovered (Fig. 4C and D). It can be observed that the energy consumption per treated volume decreases ten times for the 10-cell pair configuration compared to the single-cell pair configuration (0.24 $kWh{\cdot}m^{-3}$ and 2.63 $kWh{\cdot}m^{-3}$, respectively). Moreover, values of energy consumption for the 10-cell pair configuration in terms of N and P recovered were 7.2 $kWh{\cdot}kg^{-1}$ and 79.0 $kWh{\cdot}kg^{-1}$, respectively (7 and 3.5 times minor than in 1-cell pair experiment, respectively). It is worth emphasizing that these energy efficiencies are significantly minor than the energy consumption observed in the Haber-Bosch process, a well-established industrial process for ammonia production, which typically requires around 19.3 kWh per kilogram of nitrogen (McCarty et al., 2011) highlighting the energy efficiency achieved in this study. It is important to highlight that the stack used in this work consisted of only a maximum of 10-cell pairs of 64 cm^2 each membrane, which limits the improvement of energy consumption. Higher areas of membranes could lead to the optimization of the ED process (Voutetaki et al., 2023; Yang et al., 2023).

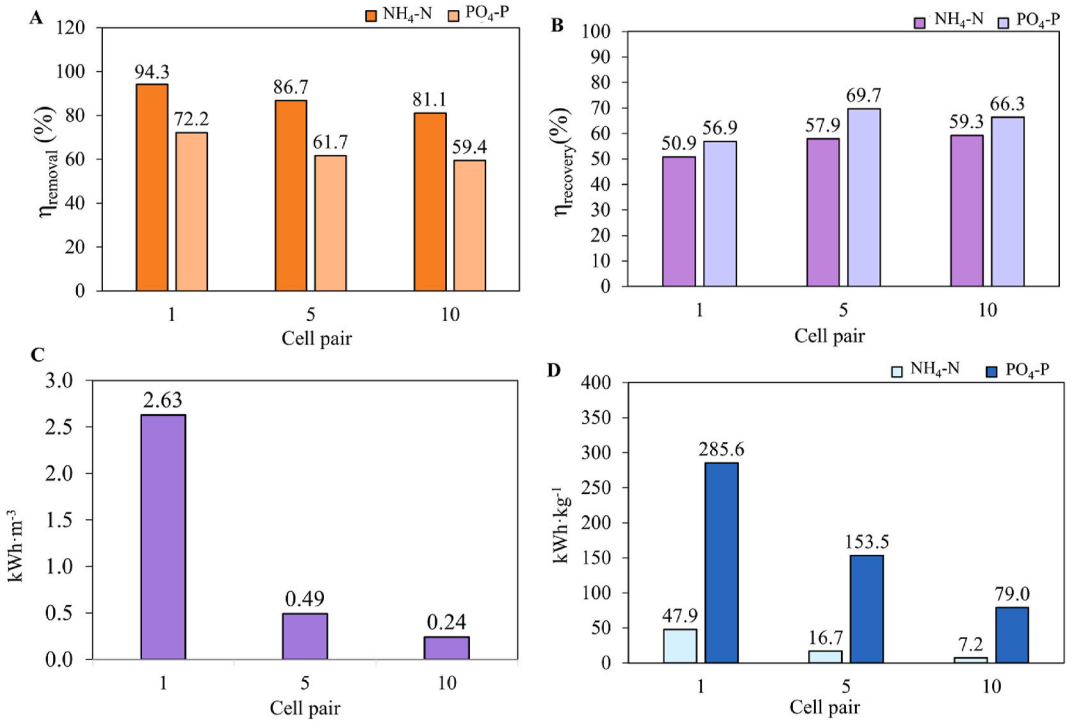

Fig. 4. Removal efficiencies (A), recovery efficiencies (B) and energy consumption (C and D) for 1, 5 and 10 cell pairs.

3.5. Effect of the power supply operating mode

This section evaluates two different operating modes of the power supply system. The first one, which has been used so far, is known as the galvanostatic mode (or constant current, CC), where a stable current is maintained while the voltage is automatically adjusted by the power supply. Under this mode, the migration velocity of the ions is controlled (Wei et al., 2022). The other mode, referred to as the potentiostatic mode (or constant voltage, CV), involves maintaining a constant voltage while the power supply automatically adjusts the current as needed. The CV mode, on the other hand, prevents the attainment of high voltage values when low concentrations are reached in the diluted compartment (Parulekar, 1998). To determine the most suitable voltage for the potentiostatic operating mode, three different voltage settings (7.5 V, 10 V, and 12.5 V) were applied using the Acid-100-OT membrane and a 10-cell pair stack configuration. The value of 7.5 V corresponds to the average initial voltage values achieved when operating in CC mode at 0.24 A (section 3.2.). Meanwhile, 10 V and 12.5 V were selected to test voltage values corresponding to currents above the working optimal current and up to the maximum current instability observed (0.33 A and 0.48 A, respectively, as discussed in section 3.2). Subsequently, these experiments were compared with the experiment showed in section 3.4, which also used the Acid-100-OT membrane and a 10-cell pair configuration but operated in the CC mode. All these experiments were conducted over four cycles to ensure a meaningful comparison and the corresponding experimental times were 191, 165, 133 and 92 min for 7.5 V, 10 V, 12.5 V and 0.24 A, respectively. Under CV mode, a cycle is completed when the current values observed for the applied voltage no longer affect the conductivity of the diluted solution. In this CV mode, an increase in the applied voltage leads also to an increase in the initial current of the cycles (Fig. S3). This results in an improvement in removal and recovery efficiencies but also in an energy consumption increase (Fig. 5C and D). Table 5 provides the average concentrations of the inlet, diluted and concentrated streams, along with the corresponding dilution and concentration ratios.

In potentiostatic experiments, higher voltages caused a marginal increase in ammonium and phosphate concentrations in the concentrated stream. For diluted stream, minimal variations occurred, except for ammonium at 7.5 V. As stated before, higher voltage levels led to shorter experiments due to the concentration polarization phenomenon. Cycle durations decreased from 50 min at 7.5 V to 40 and 30 min at 10.0 V and 12.5 V, respectively, attributed to the migration velocity increase when higher currents were applied. In the 0.24 A experiment, owing to significantly shorter operation times, lower final concentrations were achieved in the concentrated stream compared to CV experiments. This shorter time was associated with the faster attainment of critical voltages in the CC mode, leading to the concentration polarization phenomenon in the DBL of the diluted side of membrane. Dilution ratios increased at high voltages, reducing up to 30 times the ammonium inlet concentrations working at 10 V and 12.5 V. Phosphate showed minor variation across the different voltages. Concentration ratios remained constant at the three applied voltages, with final concentrations ratios around 4.6 and 3 for ammonium and phosphate, respectively. However, achieving similar concentrations required less time at higher voltages. Dilution and concentration ratios decreased for ammonium and phosphate in the 0.24 A experiment. This reduction was attributed to the lower migration velocity compared to the 10 V and 12.5 V experiments. On the other hand, as explained above, 7.5 V experiment corresponds to the average initial voltage values achieved when operating in CC mode at 0.24 A (section 3.2.). Thus, comparing both operating modes (CV at 7.5 V and CC at 0.24 A), the 0.24 A experiment exhibited shorter cycle durations resulting from early concentration polarization phenomenon. This fact contributed to a reduction in observed dilution and concentration ratios, along with lower inlet concentrations.

The removal efficiencies in the CV mode experiments (Fig. 5A) showed values exceeding 90% for ammonium and around 70% for phosphate. In CC mode, lower removal values were observed with 81.1% for ammonium and 59.40% for phosphate. This was attributed to shorter cycle durations, linked to earlier concentration polarization in the diluted compartment than in CV mode. CC mode maintains a constant ion migration rate, while in CV mode, it diminishes over the operational cycle. Recovery efficiencies (Fig. 5B) followed a similar pattern in CV experiments obtaining values around 80% and 70% for

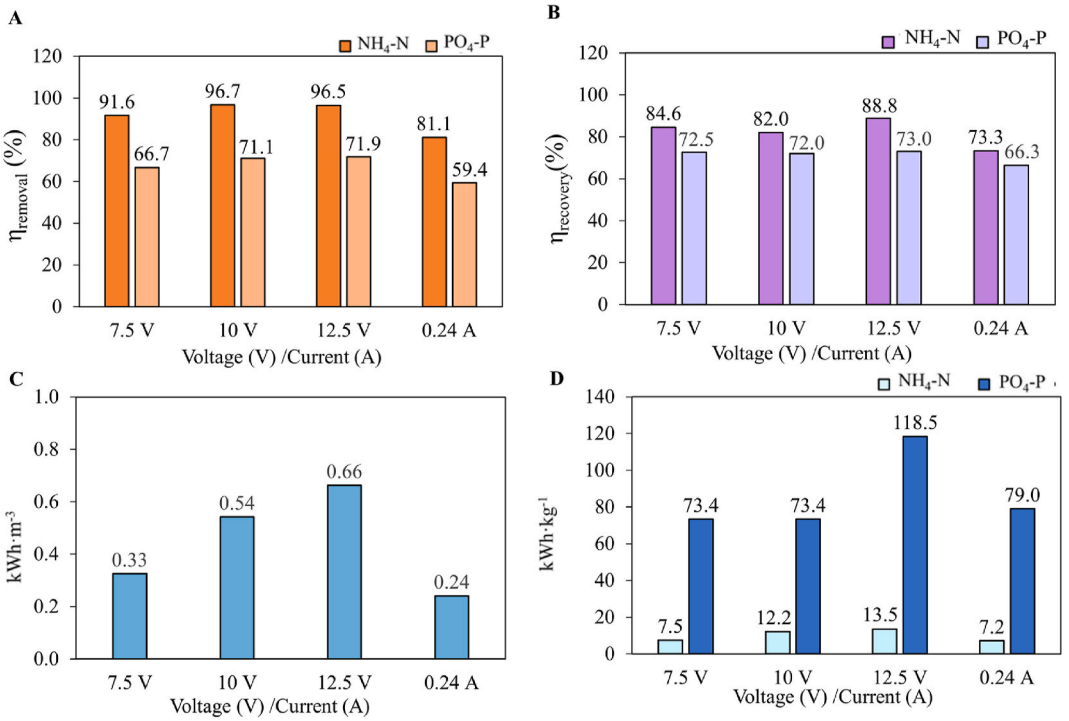

Fig. 5. Removal efficiencies (A), recovery efficiencies (B) and energy consumption (C and D) for 7.5 V, 10 V, 12.5 V and 0.24 A.

Table 5
Effect of the power supply operating mode.

	Voltage/Current	Concentration (mg/L)							Ratios	
		Inlet			Diluted			Concentrated	Dilution	Concentration
NH_4–N	7.5 V	53.62	±	1.62	3.96	±	1.31	245.39	13.5	4.6
PO_4–P		7.82	±	0.07	2.26	±	0.07	25.20	3.5	3.2
NH_4–N	10 V	54.44	±	0.05	1.59	±	0.54	252.29	34.2	4.6
PO_4–P		7.77	±	0.07	1.96	±	0.22	26.02	4.0	3.3
NH_4–N	12.5 V	56.35	±	0.00	1.72	±	0.45	278.52	32.7	4.9
PO_4–P		8.45	±	0.23	2.06	±	0.18	28.53	4.1	3.4
NH_4–N	0.24 A	51.07	±	0.45	8.41	±	0.40	191.17	6.1	3.7
PO_4–P		6.17	±	0.06	2.18	±	0.04	17.33	2.8	2.8

ammonium and phosphate, respectively. Conversely, the 0.24 A experiment resulted in lower recovery values.

In terms of energy consumption (Fig. 5C and D), significantly higher values were obtained at 10 V and 12.5 V experiments. However, when comparing the CV operating mode at 7.5 V with the CC mode at 0.24 A, similar results were achieved (0.33 $kWh{\cdot}m^{-3}$ and 0.24 $kWh{\cdot}m^{-3}$, respectively) with the latter requiring significantly less time. While CV mode at 7.5 V generally yielded better removal and recovery efficiencies than the CC mode, the time required to achieve those values was more than twice compared to the CC process (191 min for 7.5 V and 92 min for 0.24 A). As a result, the CC mode was chosen for future long-term experiments. Nevertheless, the energy consumption of the CV mode could be improved by optimizing the operating time. This implies reducing the operating time when significantly low conductivities were reached in the system not inducing significant changes in the characteristics of the streams.

3.6. Long-term experiments for stability test

A long-term experiment was carried out using the optimal parameters determined during the performance of the short-term experiments – galvanostatic (CC) mode with a current applied of 0.24 A, an Acid-100-OT AEM and a 10-cell pair configuration – to demonstrate the feasibility of the process to concentrate ammonium and phosphate for its subsequent recovery. Table 6 shows the inlet concentrations and the diluted and concentrated outlet streams concentrations of the long-term experiment. Calcium, magnesium, potassium and sulphate concentrations were determined in this experiment due to their relevance in terms of competition when working with long-term processes.

The experiment was stopped (after 7 h) when the values of the concentrated stream (740.37 mg NH_4–N/L and 50.05 mg PO_4–P/L) reached recommended PO_4–P and NH_4–N concentrations for subsequent crystallization and membrane contactor processes, respectively (Mehta et al., 2015; Noriega-Hevia et al., 2020; Salehi et al., 2018). Moreover, the experiment showed a good long-term stability (Fig. S4). In relation to the diluted stream, values for ammonium met the less restrictive discharge limits set in the Directive 91/271/EEC; however, the discharge limits for phosphate were not met. This may be attributed to the shorter time required to reach the damaged membrane voltage of 22 V in this long-term experiment, leading to reduced cycles. Further investigation is needed to improve the reduction in the concentrations of the diluted stream.

All ions presented removal efficiencies above 70% except phosphate which showed values around a 60%. This could be associated to the low migration of this ion (See Text S2). Recovery efficiencies showed values around 80% for all ions. Specifically, phosphate showed lower recovery efficiencies (62%) due to around 20% retention of this ion by the AEM, reducing the recovery efficiency. Assays to corroborate the PO_4^{-3} retention of the AEM were performed and are detailed in Text S3.

Furthermore, energy consumption values were 0.46 $kWh{\cdot}m^{-3}$ and 13.9 $kWh{\cdot}kg^{-1}$ of NH_4–N and 205.4 $kWh{\cdot}kg^{-1}$ of PO_4–P recovered. Differences between 10-cell pairs experiment, presented in section 3.4. (0.24 $kWh{\cdot}m^{-3}$, 7.2 $kWh{\cdot}kg^{-1}$ of NH_4–N and 79.0 $kWh{\cdot}kg^{-1}$ of PO_4–P), and the one conducted under the same conditions in the present section, were significative. The increased energy consumption in the long-term experiment was linked to the formation of microscaling and membrane fouling, which augmented stack resistance, resulting in elevated voltage values and consequently increased power consumption (Cao et al., 2023; Nthunya et al., 2022; Zhang et al., 2023). Similar energy consumptions were obtained by other authors that operated with similar processes. For example, Mohammadi et al. (2020) worked treating municipal wastewater with a 10-cell pair ED stack with a membrane area of 64 cm^2 to recover nitrate and obtained an energy consumption of 19.2 $kWh{\cdot}kgN^{-1}$ recovered. Nevertheless, increasing the membrane area and the number of cell pairs would enhance the values of the energy consumption. An example of this can be seen in the research conducted by Ward et al. (2018) who worked with an ED pilot scale plant with a 30-cell pair stack and a membrane effective area of 7.2 m^2 treating domestic anaerobic digester supernatant and presenting energy consumptions of 4.9 $kWh{\cdot}kg\ N^{-1}$.

Current efficiency (CE) was calculated for the long-term experiment using equation (8), yielding a value of 95%. This high CE reflects that the majority of the energy was utilized in ion migration. CE for ammonium and phosphate were determined to be 9.35% and 0.39%, respectively. The low CE value for phosphate was attributed to the low migration velocities of this ion (Table S3, Supplementary Material) and its low concentration at the inlet of the ED process.

In the present worked, it is important to note that no cleaning treatment was conducted during the long-term experiment. Therefore, implementing a cleaning treatment during the ED process could help to minimise scaling and fouling phenomena. Additionally, the use of reversal electrodialysis (EDR) – i.e., changing periodically the polarity of

Table 6
Initial and final concentrations of the long-term test with 10-cell pair configuration and efficiency values for diluted and concentrated streams.

	Concentration (mg/L)							Ratio	
	Inlet			Diluted			Concentrated	Dilution	Concentration
N–NH_4	57.11	±	6.04	11.67	±	2.85	740.37	4.9	13.0
P-PO_4	6.60	±	0.34	2.57	±	0.30	50.05	2.6	7.6
S–SO_4	98.49	±	13.45	17.48	±	9.92	1839.01	5.6	18.7
Mg^{2+}	39.81	±	0.37	10.36	±	1.83	515.62	3.8	13.0
Ca^{2+}	156.81	±	1.10	29.70	±	6.22	2135.66	5.3	13.6
K^+	9.66	±	0.44	1.98	±	0.47	127.62	4.9	13.2

the electrodes during the ED performance – might offer an alternative to prevent scaling concerns (Shi et al., 2019; Turek and Dydo, 2003). Further research is necessary to explore these possibilities and to reduce energy consumption in long-term experiments.

4. Conclusions

The results of this research demonstrate the feasibility of using ED technology to concentrate ammonium and phosphate from real wastewater coming from the effluent of an AnMBR. Short-term experiments indicated that a 10-cell pair stack operating in galvanostatic mode at 0.24 A, using an Acid-100-OT AEM, was the most suitable combination for the concentration of ammonium and phosphate during the ED process. Finally, a long-term experiment was conducted to assess the feasibility of the process with the selected parameters. Promising results with concentrations of up to 740 mg/L of NH_4–N and 50 mg/L of PO_4–P in 7 h of operation were achieved. The study identified two bottlenecks that need further investigation: the increase in energy consumption due to scaling and fouling and the failure in achieving the discharge limits in the diluted stream. Future research will address these issues.

CRediT authorship contribution statement

P. Ruiz-Barriga: Writing – original draft, Methodology, Investigation, Formal analysis, Conceptualization. **J. Serralta:** Writing – review & editing, Funding acquisition. **A. Bouzas:** Writing – review & editing, Supervision, Funding acquisition, Conceptualization. **J. Carrillo-Abad:** Writing – review & editing, Supervision, Conceptualization.

Declaration of competing interest

The authors declare that they have no known competing financial interests or personal relationships that could have appeared to influence the work reported in this paper.

Data availability

Data will be made available on request.

Acknowledgements

This research work has been supported by the Spanish Ministry of Science and Innovation by “RECREATE” (PID2020-114315RB-C21/22) and “MEM4REC” (CTM2017-86751-C2-1/2-R) projects, jointly with the European Regional Development Fund (ERDF), which are gratefully acknowledged.

Appendix A. Supplementary data

Supplementary data to this article can be found online at https://doi.org/10.1016/j.jenvman.2024.121712.

Page1 | 1.

References

Al-Amshawee, S., Bin, Y., Yunus, M., Aziz, A., Azoddein, M., Hassell, D.G., Habib Dakhil, I., Hasan, H.A., 2019. Electrodialysis desalination for water and wastewater: a review. https://doi.org/10.1016/j.cej.2019.122231.

Cao, Y., Li, X., Zhang, L., 2023. Construction of bipolar membrane electrodialysis reactor for removal and recovery of nitrogen and phosphorus from wastewater. Int. J. Electrochem. Sci. 18, 100051 https://doi.org/10.1016/j.ijoes.2023.100051.

Cerva, M. La, Gurreri, L., Tedesco, M., Cipollina, A., Ciofalo, M., Tamburini, A., Micale, G., 2018. Determination of limiting current density and current efficiency in electrodialysis units. https://doi.org/10.1016/j.desal.2018.07.028.

Cowan, D.A., Brown, J.H., 1959. Effect of Turbulence on limiting current in electrodialysis cells. Ind. Eng. Chem. 51, 1445–1448. https://doi.org/10.1021/ie50600a026.

Darestani, M., Haigh, V., Couperthwaite, S.J., Millar, G.J., Nghiem, L.D., 2017. Hollow fibre membrane contactors for ammonia recovery: current status and future developments. https://doi.org/10.1016/j.jece.2017.02.016.

Desmidt, E., Ghyselbrecht, K., Monballiu, A., Rabaey, K., Verstraete, W., Meesschaert, B. D., 2013. Factors influencing urease driven struvite precipitation. https://doi.org/10.1016/j.seppur.2013.03.010.

González-Camejo, J., Barat, R., Ruano, M.V., Seco, A., Ferrer, J., 2018. Outdoor flat-panel membrane photobioreactor to treat the effluent of an anaerobic membrane bioreactor. Influence of operating, design, and environmental conditions. Water Sci. Technol. 78, 195–206. https://doi.org/10.2166/wst.2018.259.

He, G.-X., He, L.-H., Zhao, Z.-W., Chen, X.-Y., Gao, L.-L., Liu, X.-H., 2013. Thermodynamic study on phosphorus removal from tungstate solution via magnesium salt precipitation method. Trans. Nonferrous Met. Soc. China 23, 3440–3447. https://doi.org/10.1016/S1003-6326(13)62886-1.

Herrera, A., D'Imporzano, G., Acién Fernandez, F.G., Adani, F., 2021. Sustainable production of microalgae in raceways: nutrients and water management as key factors influencing environmental impacts. J. Clean. Prod. 287 https://doi.org/10.1016/J.JCLEPRO.2020.125005.

Isaacson, M.S., Sonin, A.A., 1976. Sherwood number and Friction factor correlations for electrodialysis systems, with application to process optimization. Ind. Eng. Chem. Process Des. Dev. 15, 313–321. https://doi.org/10.1021/i260058a017.

Luo, W., Hai, F.I., Price, W.E., Guo, W., Ngo, H.H., Yamamoto, K., Nghiem, L.D., 2016. Phosphorus and water recovery by a novel osmotic membrane bioreactor–reverse osmosis system. Bioresour. Technol. 200, 297–304. https://doi.org/10.1016/J.BIORTECH.2015.10.029.

Luther, A.K., Desloover, J., Fennell, D.E., Rabaey, K., 2015. Electrochemically driven extraction and recovery of ammonia from human urine. Water Res. https://doi.org/10.1016/j.watres.2015.09.041.

Martí-Calatayud, M.C., 2015. Ceramic anion-exchange membranes based on microporous supports infiltrated with hydrated zirconium dioxide Enhanced Reader. RSC Adv. 46348–46358.

Martí-Calatayud, M.C., García-Gabaldón, M., Pérez-Herranz, V., 2018a. Mass transfer phenomena during electrodialysis of multivalent ions: chemical equilibria and overlimiting currents. Appl. Sci. 8 https://doi.org/10.3390/app8091566.

Martí-Calatayud, M.C., García-Gabaldón, M., Pérez-Herranz, V., 2018b. Mass transfer phenomena during electrodialysis of multivalent ions: chemical equilibria and overlimiting currents. Appl. Sci. 8 https://doi.org/10.3390/app8091566.

McCarty, P.L., Bae, J., Kim, J., 2011. Domestic wastewater treatment as a net energy producer-can this be achieved? Environ. Sci. Technol. 45, 7100–7106. https://doi.org/10.1021/ES2014264.

Mehta, C.M., Khunjar, W.O., Nguyen, V., Tait, S., Batstone, D.J., 2015. Technologies to recover nutrients from waste streams: a critical review. Crit. Rev. Environ. Sci. Technol. 45, 385–427. https://doi.org/10.1080/10643389.2013.866621.

Mohammadi, R., Ramasamy, D.L., Sillanpää, M., 2020. Enhancement of nitrate removal and recovery from municipal wastewater through single-and multi-batch electrodialysis: process optimisation and energy consumption. https://doi.org/10.1016/j.desal.2020.114726.

No, L., 1991. Council Directive 91/271 EEC. The Council of the European Communities.

Noriega-Hevia, G., Serralta, J., Borrás, L., Seco, A., Ferrer, J., 2020. Nitrogen recovery using a membrane contactor: modelling nitrogen and pH evolution Ammonia recovery pH modelling Nitrogen recovery modelling Membrane contactor for nitrogen recovery Nutrient recovery from anaerobic digestion. https://doi.org/10.1016/j.jece.2020.103880.

Nthunya, L.N., Bopape, M.F., Mahlangu, O.T., Mamba, B.B., Van der Bruggen, B., Quist-Jensen, C.A., Richards, H., 2022. Fouling, performance and cost analysis of membrane-based water desalination technologies: a critical review. J. Environ. Manag. 301, 301–4797. https://doi.org/10.1016/J.JENVMAN.2021.113922.

Osset-Álvarez, M., Rovira-Alsina, L., Pous, N., Blasco-Gómez, R., Colprim, J., Dolors Balaguer, M., Puig, S., 2019. Niches for bioelectrochemical systems on the recovery of water, carbon and nitrogen in wastewater treatment plants. https://doi.org/10.1016/j.biombioe.2019.105380.

Parulekar, S.J., 1AD. Optimal Current and Voltage Trajectories for Minimum Energy Consumption in Batch Electrodialysis.

Pastor, L., Mangin, D., Ferrer, J., Seco, A., 2009. Struvite formation from the supernatants of an anaerobic digestion pilot plant. Bioresour. Technol. 101, 118–125. https://doi.org/10.1016/j.biortech.2009.08.002.

Raychaudhuri, A., Behera, M., 2021. Nutrient removal and recovery in bioelectrochemical systems. Delivering Low-Carbon Biofuels with Bioproduct Recovery: an Integrated Approach to Commercializing Bioelectrochemical Systems, pp. 45–83. https://doi.org/10.1016/B978-0-12-821841-9.00001-3.

Robles, Á., Ruano, M.V., Charfi, A., Lesage, G., Heran, M., Harmand, J., Seco, A., Steyer, J.P., Batstone, D.J., Kim, J., Ferrer, J., 2018. A review on anaerobic membrane bioreactors (AnMBRs) focused on modelling and control aspects. Bioresour. Technol. https://doi.org/10.1016/j.biortech.2018.09.049.

Rongwong, W., Goh, K., 2020. Resource recovery from industrial wastewaters by hydrophobic membrane contactors: a review. J. Environ. Chem. Eng. 8, 104242 https://doi.org/10.1016/J.JECE.2020.104242.

Salehi, S., Cheng, K.Y., Heitz, A., Ginige, M.P., 2018. Re-visiting the Phostrip process to recover phosphorus from municipal wastewater. Chem. Eng. J. 343, 390–398. https://doi.org/10.1016/J.CEJ.2018.02.074.

Sedighi, M., Mahdi, M., Usefi, B., Fauzi Ismail, A., Ghasemi, M., 2022. Environmental sustainability and ions removal through electrodialysis desalination: operating conditions and process parameters. https://doi.org/10.1016/j.desal.2022.116319.

Sena, M., Hicks, A., 2018. Life cycle assessment review of struvite precipitation in wastewater treatment. https://doi.org/10.1016/j.resconrec.2018.08.009.

Shi, L., Xie, S., Hu, Z., Wu, G., Morrison, L., Croot, P., Hu, H., Zhan, X., 2019. Nutrient recovery from pig manure digestate using electrodialysis reversal: membrane fouling and feasibility of long-term operation. J. Membr. Sci. 573, 560–569. https://doi.org/10.1016/J.MEMSCI.2018.12.037.

Simões, C., Vital, B., Sleutels, T., Saakes, M., Brilman, W., 2022. Scaled-up multistage reverse electrodialysis pilot study with natural waters. Chem. Eng. J. 450, 138412 https://doi.org/10.1016/J.CEJ.2022.138412.

Singh, R., Hankins, N.P., 2016. Introduction to membrane processes for water treatment. Emerging Membrane Technology for Sustainable Water Treatment 15–52. https://doi.org/10.1016/B978-0-444-63312-5.00002-4.

Strathmann, H., 2010. Electrodialysis, a mature technology with a multitude of new applications. Desalination. https://doi.org/10.1016/j.desal.2010.04.069.

Tansel, B., Lunn, G., Monje, O., 2018. Struvite formation and decomposition characteristics for ammonia and phosphorus recovery: a review of magnesium-ammonia-phosphate interactions. Chemosphere 194, 504–514. https://doi.org/10.1016/J.CHEMOSPHERE.2017.12.004.

Tarpeh, W.A., Barazesh, J.M., Cath, T.Y., Nelson, K.L., 2018. Electrochemical stripping to recover nitrogen from source-separated urine. Environ. Sci. Technol. 52, 1453–1460. https://doi.org/10.1021/acs.est.7b05488.

Turek, M., Dydo, P., 2003. Electrodialysis reversal of calcium sulphate and calcium carbonate supersaturated solution. Desalination 158, 91–94. https://doi.org/10.1016/S0011-9164(03)00438-7.

Ukwuani, A.T., Tao, W., 2016. Developing a vacuum thermal stripping e acid absorption process for ammonia recovery from anaerobic digester effluent. https://doi.org/10.1016/j.watres.2016.09.054.

Vega, E., Paredes, L., Marks, E.A.N., Singla, B., Castaño-Sánchez, O., Casas, C., Vilaplana, R., Mora, M., Ponsá, S., Llenas, L., 2022. Application of vibrating reverse osmosis technology for nutrient recovery from pig slurry in a circular economy model. Membranes 12. https://doi.org/10.3390/membranes12090848.

Voutetaki, A., Plakas, K.V., Papadopoulos, A.I., Bollas, D., Parcharidis, S., Seferlis, P., 2023. Pilot-scale separation of lead and sulfate ions from aqueous solutions using electrodialysis: application and parameter optimization for the battery industry. J. Clean. Prod. 410, 137200 https://doi.org/10.1016/j.jclepro.2023.137200.

Ward, A.J., Arola, K., Thompson Brewster, E., Mehta, C.M., Batstone, D.J., 2018. Nutrient recovery from wastewater through pilot scale electrodialysis. Water Res. https://doi.org/10.1016/j.watres.2018.02.021.

Wei, C.-Y., Pan, S.-Y., Lin, Y.-I., Ngoc, T., Cao, D., 2022. Anaerobic swine digestate valorization via energy-efficient electrodialysis for nutrient recovery and water reclamation. https://doi.org/10.1016/j.watres.2022.119066.

Xie, M., Shon, H.K., Gray, S.R., Elimelech, M., 2016. Membrane-based processes for wastewater nutrient recovery: technology, challenges, and future direction. Water Res. https://doi.org/10.1016/j.watres.2015.11.045.

Yan, H., Wang, Y., Wu, L., Shehzad, M.A., Jiang, C., Fu, R., Liu, Z., Xu, T., 2018. Multistage-batch electrodialysis to concentrate high-salinity solutions: process optimisation, water transport, and energy consumption. https://doi.org/10.1016/j.memsci.2018.10.008.

Yan, T., Ye, Y., Ma, H., Zhang, Y., Guo, W., Du, B., Wei, Q., Wei, D., Ngo, H.H., 2018. A critical review on membrane hybrid system for nutrient recovery from wastewater. Chem. Eng. J. https://doi.org/10.1016/j.cej.2018.04.166.

Yang, D., Liu, H., She, Q., 2023. Mixed cation transport behaviours in electrodialysis during simultaneous ammonium enrichment and wastewater desalination. Desalination 545. https://doi.org/10.1016/j.desal.2022.116155.

Ye, Y., Hao Ngo, H., Guo, W., Liu, Yiwen, Li, J., Liu, Yi, Zhang, X., Jia, H., Barcelo, D., Ngo, H.H., 2017. Insight into chemical phosphate recovery from municipal wastewater. Sci. Total Environ. 576, 159–171. https://doi.org/10.1016/j.scitotenv.2016.10.078.

Ye, Z.L., Ghyselbrecht, K., Monballiu, A., Pinoy, L., Meesschaert, B., 2019. Fractionating various nutrient ions for resource recovery from swine wastewater using simultaneous anionic and cationic selective-electrodialysis. Water Res. https://doi.org/10.1016/j.watres.2019.05.085.

Zhang, M., Xia, Q., Zhao, X., Guo, J., Zeng, L., Zhou, Z., 2023. Concentration effects of calcium ion on polyacrylamide fouling of ion-exchange membrane in electrodialysis treatment of flue gas desulfurization wastewater. Sep. Purif. Technol. 304, 122383 https://doi.org/10.1016/J.SEPPUR.2022.122383.

Zhang, Y., Desmidt, E., Van Looveren, A., Pinoy, L., Meesschaert, B., Van Der Bruggen, B., 2013. Phosphate separation and recovery from wastewater by novel electrodialysis. Environ. Sci. Technol. 47, 5888–5895. https://doi.org/10.1021/es4004476.